

1    **Replication of detector simulations using supervised machine**  
2                                    **learning**

3            D. Benjamin, S. Chekanov, W. Hopkins, Y. Li, J. R. Love,  
4                            *HEP Division, Argonne National Laboratory,*  
5                            *9700 S. Cass Avenue, Argonne, IL 60439, USA*

6                            (Dated: May 9, 2019)

Abstract

## 7 I. ACTION ITEMS FOR EDITORS

- 8     • What  $R$ -parameter are we using?  $R = 0.4$  or  $R = 0.5$ ? (Sergei)
- 9     • Sergei and Walter need to check they are doing the same matching of truth and reco  
10       jets (what is the  $\Delta R$ ?). (Sergei/Walter)
- 11    • Need to align parameters of unbinned and binned NNs. (Sergei/Walter)
  - 12       – Why are we using different activation functions (ReLU vs sigmoid) in the hidden  
13         layers?
  - 14       – Why do we have different dimensions for the output 100 vs 200?
  - 15       – For the unbinned preprocessing, are we removing resolution outliers?
- 16    • Fix missing references (Doug).
  - 17       – ReLU reference?
  - 18       – Madgraph reference (can take this from stop0L paper)?
- 19    • Write something about the hyperparameters (Ying).
  - 20       – Maybe rerun the hyperparameter scan again?
- 21    • Normalize binned NN  $\eta$  comparison histograms to really see shape differences.
- 22    • Write conclusion (Jeremy)
  - 23       – Focus on truth smearing replacement and how this is automated.
- 24    • Should we add CPU performance comparison?
  - 25       – TruthSmearingFunctions for 1M jets vs our method?
- 26    • Should we do a MET and mt comparison?
  - 27       – This really only makes sense within ATLAS.

## 28 II. INTRODUCTION

29 A cornerstone of particle collision experiments is Monte Carlo (MC) simulations of physics  
30 processes followed by simulations of detector responses. With increased complexity of such  
31 experiments, such as those at the Large Hadron Collider (LHC), the detector simulations  
32 become increasing complex and time consuming. For example, the time required to simulate  
33 Geant4 hits [1] and to reconstruct from such hits physics objects (electrons, muons, taus, jets)  
34 requires a factor 100-1000 more CPU time than the creation of typical Monte Carlo events  
35 that represent physics processes according to theoretical models (“truth level” MC event  
36 generation). A possible method to speed up simulations of detector responses is to apply  
37 neural networks (NN) trained using the actual Geant4-based simulations, and use such  
38 supervised NN for transforming truth-level MC objects (jets and other identified particles)  
39 to objects modified by detectors (“detector-level”).

40 A typical simulation of detector response stochastically modifies positions and energies  
41 of particles and jets created by MC generators at the “truth-level”. Another important  
42 component of such simulations is to introduce additional particles due to misconstruing  
43 energy deposits in active detector volumes (examples include misreconstructed electrons or  
44 photons which are, in fact, hadronic jets, etc.). The latter effects represent a significant com-  
45 plication for the so-called “fast” or “parameterized” detector simulations, such as Delphes  
46 [2]. Nevertheless, fast simulations is proven to be a vital tools for physics performance  
47 studies.

48 One advantage of fast simulations based on machine learning is that the neural net-  
49 works can automatically learn the features introduced by detailed full simulations, therefore,  
50 handcrafting smearing parameters represent resolutions and inefficiencies, as it was done in  
51 Delphes and other fast simulations, is not required. A neural network trained using realistic  
52 detector simulation should memorize the transformation from the truth-level to the detector  
53 level without interference from analyzers. Another advantage is that the NN approach can  
54 introduce a complex interdependence of variables which is currently difficult to implements  
55 in parameterized fast simulations. Finally, we expect that NN approach will be faster than  
56 the current fast simulations (this will be described later).

57 As a first step towards fast detector simulations using machine learning techniques, it  
58 is instructive to investigate how a transformation from the “truth-level” MC to “detector-

level” objects can be performed, leaving aside the question of introducing objects that are created by misreconstructions.

### III. TRADITIONAL PARAMETERIZED FAST SIMULATIONS

In abstract terms, a typical variable  $f_i$  that characterizes a particle/jet, such as transverse momentum ( $p_T$ ), pseudorapidity ( $\eta$ ), can be viewed as a multivariate transform  $F$  of the original variable  $\xi_1^T$  at truth-level:

$$\xi_1 = F(\xi_1^T, \xi_2^T, \xi_3^T, \dots, \xi_N^T).$$

Generally, such a transform depends on several other variables  $\xi_2^T \dots \xi_N^T$  characterizing this (or other) objects at the truth level. For example, the extent at which jet transverse momentum,  $p_T$  is modified by a detector depends on the original truth-level transverse momentum ( $\xi_1^T = p_T^T$ ), pseudorapidity  $\eta$ , flavor of jets and other effects that can be inferred from the truth level. For example, if particular detector modules in the azimuthal angle ( $\phi$ ) are not active, this would introduce an additional dependence of this transform on  $\phi$ . Typical fast (“parameterized”) simulations ignores the full range of correlations between the variables. In most cases, the above transform is reduced to a single variable, or two (as in the case of Delphes fast simulations where energy resolution of clusters depend on the original energies of particles and their positions in  $\eta$ ). In order to take into account correlations between multiple parameters characterizing transformations to the detector level, the following steps have to be undertaken:

- create a grid in the hypercube with the dimension  $N_b^N$ , where  $N_b$  is the number of histogram bins for the distributions  $f_1 - f_i^N$  representing “resolution” smearing. This can be done numerically, using frequencies, or using analytically using “resolution functions”.
- calculate “efficiencies” that model losses of particles/jets for each variable.

It should be pointed that the calculation speed for parameterized fast simulations of one variable that depends on  $N$  other variables at the truth level depends as  $N_b^N$  since each object at the truth level should be placed inside the grid defined by  $N_b$  bins. Therefore, complex parameterisations of resolutions and efficiency’s for  $N > 2$  becomes CPU intensive.

#### 86 IV. MACHINE LEARNING APPROACH FOR FAST SIMULATION

87 Unlike the traditional approach for fast simulation using parameterized density functions  
 88 for resolution variables and probability values for efficiency, a neural network approach  
 89 offers an opportunity to formulate this problem in terms of neural-network nodes and their  
 90 connections that scale as  $N_b^N \cdot N$ , which can speed up the fast simulations and, at the same  
 91 time, can be used for learning more complex full simulations in an automated way.

92 In the case of objects, such as jets, a typical truth-level input are jet transverse momen-  
 93 tum,  $\eta$ ,  $\phi$  and jet mass  $m$ , while the output is an array of output nodes that represent the  
 94 binned probability density function (pdf) of the resolution for a single variable (such as jet  
 95  $p_T$ ). The output can also include a node that specifies the efficiency, i.e. a variable that is  
 96 either 0 (e.g. a jet did not pass the detector acceptance) or 1 (a jet was within the detector  
 97 acceptance). Additional input variables can be jet flavor at the truth level, jet radius etc.,  
 98 i.e. any variable that can influence the output of such neural network. Figure 1 shows a  
 99 schematic representation of the NN architecture for modelling detector response for a single  
 100 output variable. In this example, we show a single hidden layer (in principle, the NN can  
 101 also be deep with several hidden layers)

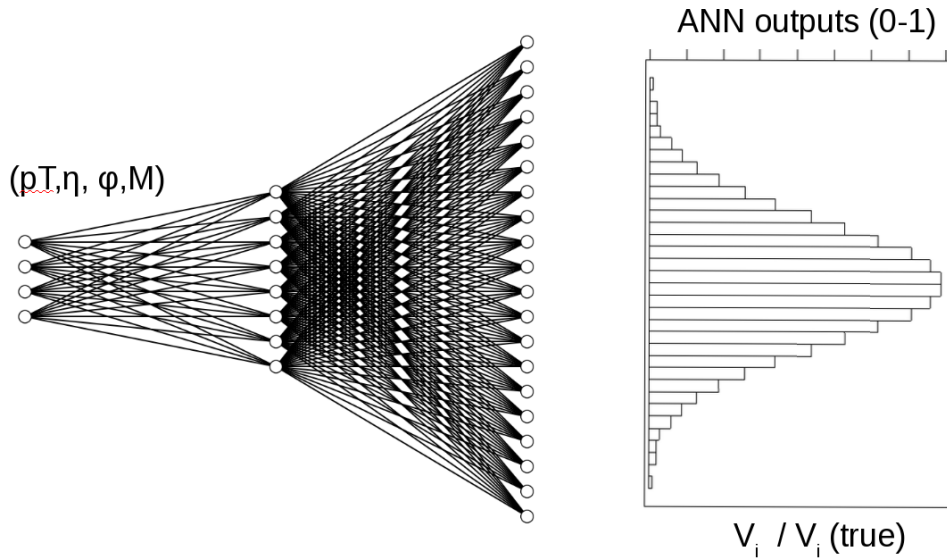


FIG. 1. A schematic representation of the NN architecture for modelling the detector response to truth-level input variables.

## 102 V. MONTE CARLO SIMULATED EVENT SAMPLES

103 Monte Carlo events used for this analysis were generated using the Madgraph generator [?]   
 104 ]. The simulated process was  $t\bar{t} + jets$ , which give a high rate of jets and lepton. In   
 105 addition, multijet events were added to increase the statistics at high  $p_T$  jets. Hadronic jets   
 106 were reconstructed with the FASTJET package [?] using the anti- $k_T$  algorithm [?] with a   
 107 distance parameter of 0.5. The detector simulation was performed with the Delphes package   
 108 [?] with the ATLAS-like detector geometry. The event samples used in this paper, before   
 109 and after the fast simulation, are available from the HepSim database [?]. In this paper   
 110 only the transformation from truth-level jets to detector-level jets was performed, however   
 111 the methodology should be object agnostic.

112 The distributions of quantities used as the input for the NN,  $p_T$ ,  $\eta$ ,  $\phi$ ,  $m$ , are shown in   
 113 Figure 2.

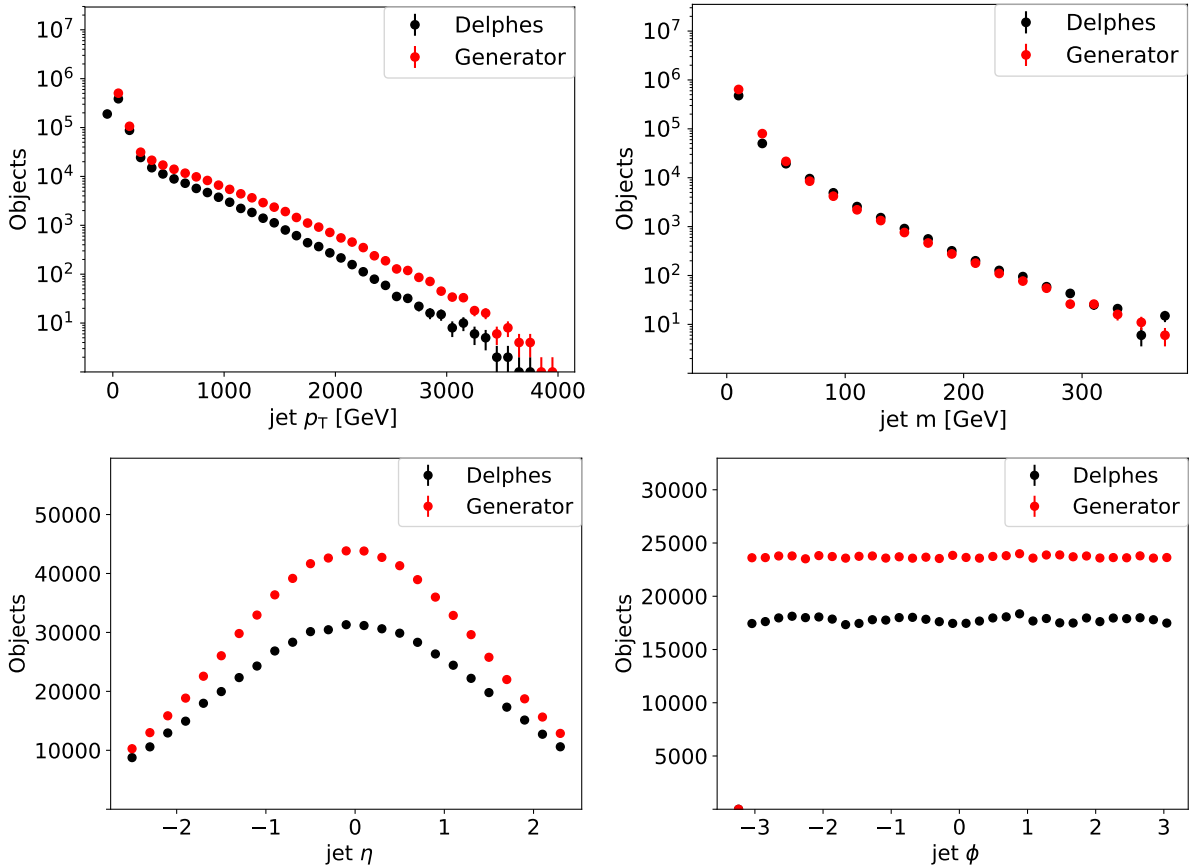


FIG. 2. Input variable shapes for truth-level (red) and detector-level quantities (black).

114 To facilitate gradient descent in all direction of the input variables, the input variables  
 115 are all scaled to be in the range  $[0,1]$ . This avoids the  $p_T$  and the mass from having a  
 116 disproportional affect on the training of the NNs. The output variables, consisting  $p_T^{\text{truth}} -$   
 117  $p_T^{\text{reco}}$ ,  $\eta^{\text{truth}} - \eta^{\text{reco}}$ ,  $\phi^{\text{truth}} - \phi^{\text{reco}}$ ,  $m^{\text{truth}} - m^{\text{reco}}$ , are also scaled to have values between 0 and  
 118 1 and are shown in Figure 3. Only object that are within the 1<sup>st</sup> and 99<sup>th</sup> percentile of each  
 119 of the resolution distributions are considered in this study since objects outside this range  
 120 are typically not used in physics analyses.

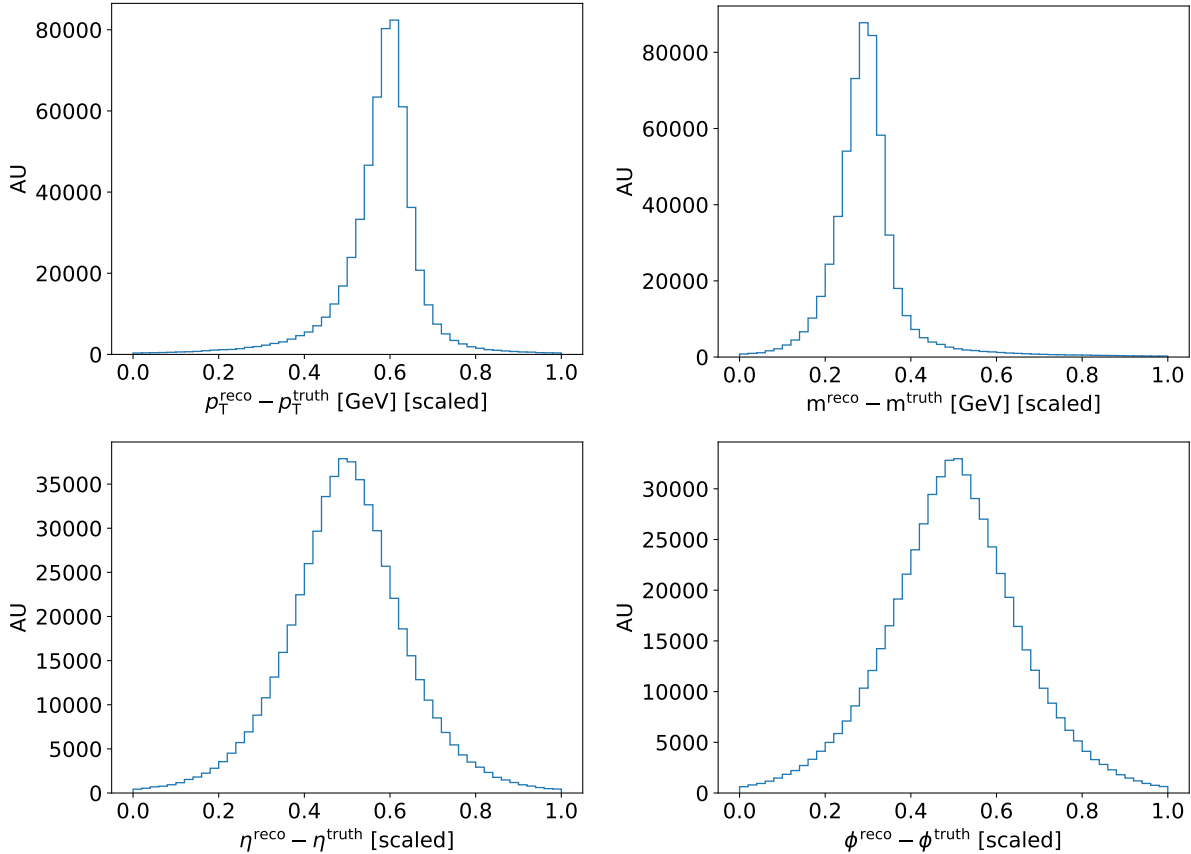


FIG. 3. Differences between truth-level and detector-level quantities after scaling so that the difference is in the range  $[0,1]$ .

## 121 VI. NEURAL NETWORK STRUCTURES

122 Two approaches when using the input variables are considered: one bins the input vari-  
 123 ables into 20 bins for each variable (we will called this the “binned NN”) while the other  
 124 leaves the input variables unbinned (this will be referred to as the “unbinned NN”. For the

125 binned case, the network structure consists of an input layer with  $4 \times 20$  nodes, one fully con-  
 126 nected hidden layer with 100 nodes and an output layer with 201 nodes. The first 200 nodes  
 127 represent the bins in jet resolution  $(p_T^{\text{truth}} - p_T^{\text{reco}}, \eta^{\text{truth}} - \eta^{\text{reco}}, \phi^{\text{truth}} - \phi^{\text{reco}}, m^{\text{truth}} - m^{\text{reco}})$ ,  
 128 and one node is added, which either has a value of 0 and 1, represents the probability that  
 129 the given input jet passes the detector acceptance and reconstruction. The binning of the  
 130 output reduces a regression problem to a multi-categorization problem which simplifies and  
 131 reduces the required network parameters. The NN uses sigmoid activation function for all  
 132 layers. After the training, the output NN nodes contain 201 values representing the proba-  
 133 bility density distribution for the jet resolution function which can be used to generate shifts  
 134 in the truth-level quantity due to the detector smearing effects.

135 In the case of the unbinned inputs, the outputs are binned to have 101 bins with the first  
 136 bin for the first feature representing the acceptance and reconstruction inefficiency, similar to  
 137 the binned NN case. **mention what happens when there are multiple truth jets within a reco**  
 138 **jet**. The binned output variables are shown in Figure 3. As with the binned NN, an NN is  
 139 trained for each feature, i.e. an NN exists for  $p_T$ ,  $m$ ,  $\eta$ , and  $\phi$ , individually, resulting in four  
 140 NNs. The binned NNs consist of five layers with 100 nodes with each node having a ReLu  
 141 [cite relu] activation function. The output layer has 101 nodes with a softmax activation  
 142 function. The NN is trained over 20 epochs with batch size 1000.

## 143 VII. RESULTS

144 The results for the binned NN training compared to the default Delphes fast simulation  
 145 (used for the NN training) are shown in Fig. ???. To test whether the NN learned correlations  
 146 between input parameters and the resolutions, the jets were divided into central ( $|\eta| < 2$   
 147 and forward ( $|\eta| > 2$ ) jets, then the  $p_T$  resolutions were compared between the two regions  
 148 for both the Delphes jets as well as the NN-generated jets. These two regions in detectors  
 149 typically have different jet  $p_T$  resolutions and thus the  $p_T$  resolution is correlated with the  $\eta$ .  
 150 The trained binned NN describes the Delphes simulations well. In particular, the dependence  
 151 of jet  $p_T$  resolution is well modeled for different  $\eta$  regions, which is an indication that the  
 152 NN learns correlations between input variables. It is also important to note that the jet  
 153 efficiency included in Delphes can be reproduced by the NN with a 1% accuracy.

154 The learned resolution pdfs learned by the unbinned NN are compared to the Delphes



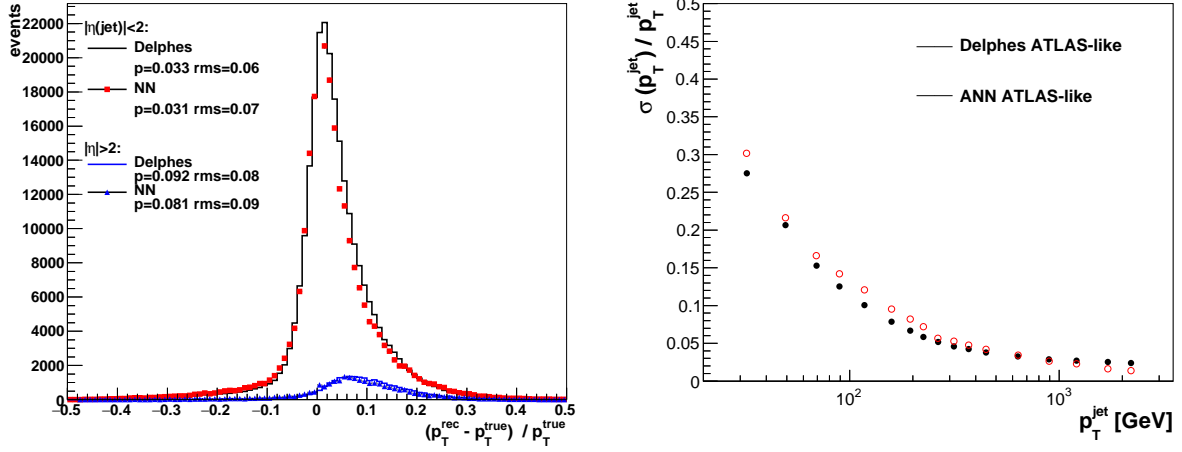


FIG. 4. Left: NN-generated jet  $p_T$  resolutions for central (black) and forward (red) jets for Delphes (circles) and NN-generated jets (dashed line). Right: The standard deviation of the  $p_T^{\text{truth}} - p_T^{\text{reco}}$  as a function of  $p_T$  for Delphes (black) and the NN (red).

resolutions in Fig. 5.

The truth-level quantities are corrected using the NN generated pdfs resulting in NN generated objects. A comparison between truth-level, detector-level, and NN-generated features is shown in Fig. 6. The agreement between detector-level and NN-generated features is within XX%. As with the binned NN, figure 7 shows that the NN reproduces the difference in resolutions for central and forward jets.

## VIII. HYPERPARAMETER SCAN

## IX. PERFORMANCE CONSIDERATION?

For the binned NN, the training of one variable typically takes 30 min using 16 parallel processes.

## X. CONCLUSION

## ACKNOWLEDGMENTS

The submitted manuscript has been created by UChicago Argonne, LLC, Operator of Argonne National Laboratory (“Argonne”). Argonne, a U.S. Department of Energy Office

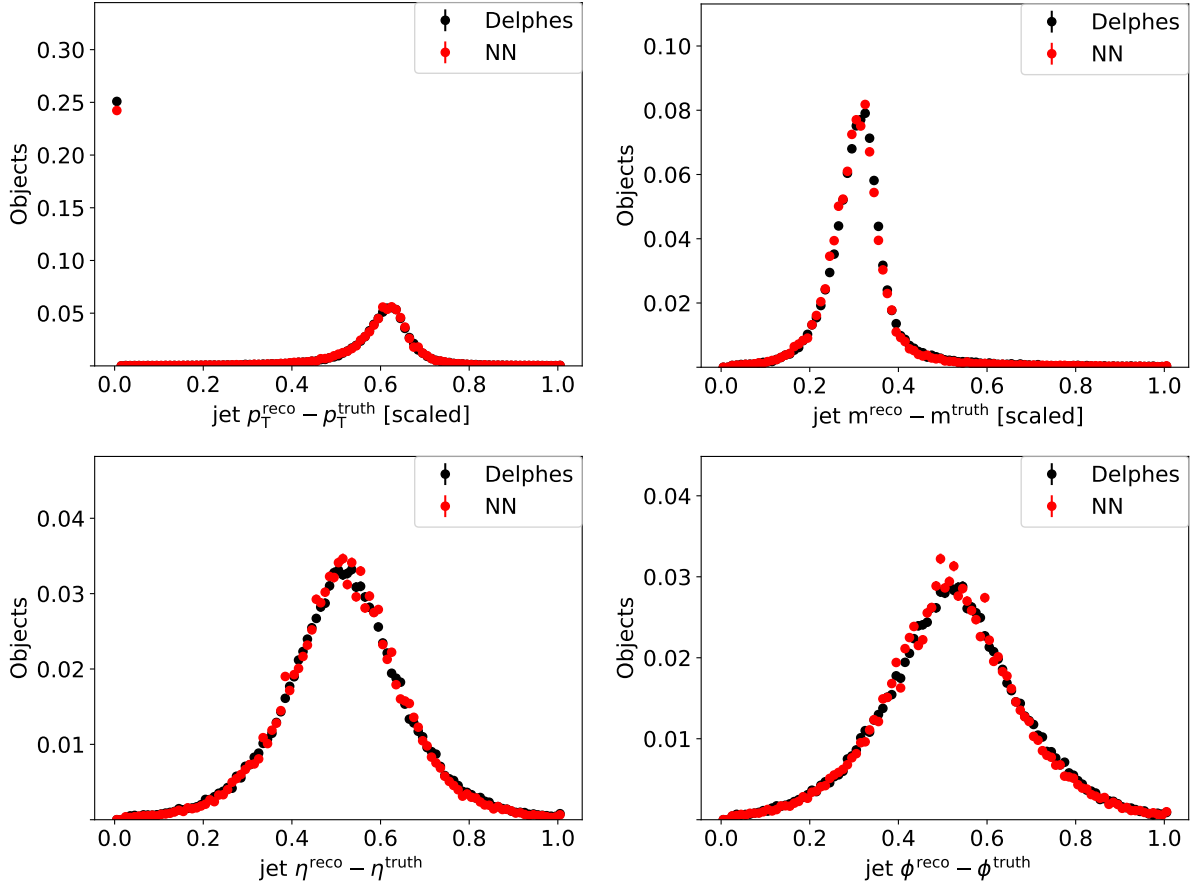


FIG. 5. Resolutions for the jet  $p_T$ , mass,  $\eta$ ,  $\phi$ . The red dots correspond to the NN output summed over the entire test sample while the black dots correspond to resolutions from Delphes. The first bin of the  $p_T$  pdf is used to quantify the inefficiency of the reconstruction.

of Science laboratory, is operated under Contract No. DE-AC02-06CH11357. The U.S. Government retains for itself, and others acting on its behalf, a paid-up nonexclusive, irrevocable worldwide license in said article to reproduce, prepare derivative works, distribute copies to the public, and perform publicly and display publicly, by or on behalf of the Government. The Department of Energy will provide public access to these results of federally sponsored research in accordance with the DOE Public Access Plan. <http://energy.gov/downloads/doe-public-access-plan>. Argonne National Laboratory's work was funded by the U.S. Department of Energy, Office of High Energy Physics under contract DE-AC02-06CH11357.

## REFERENCES

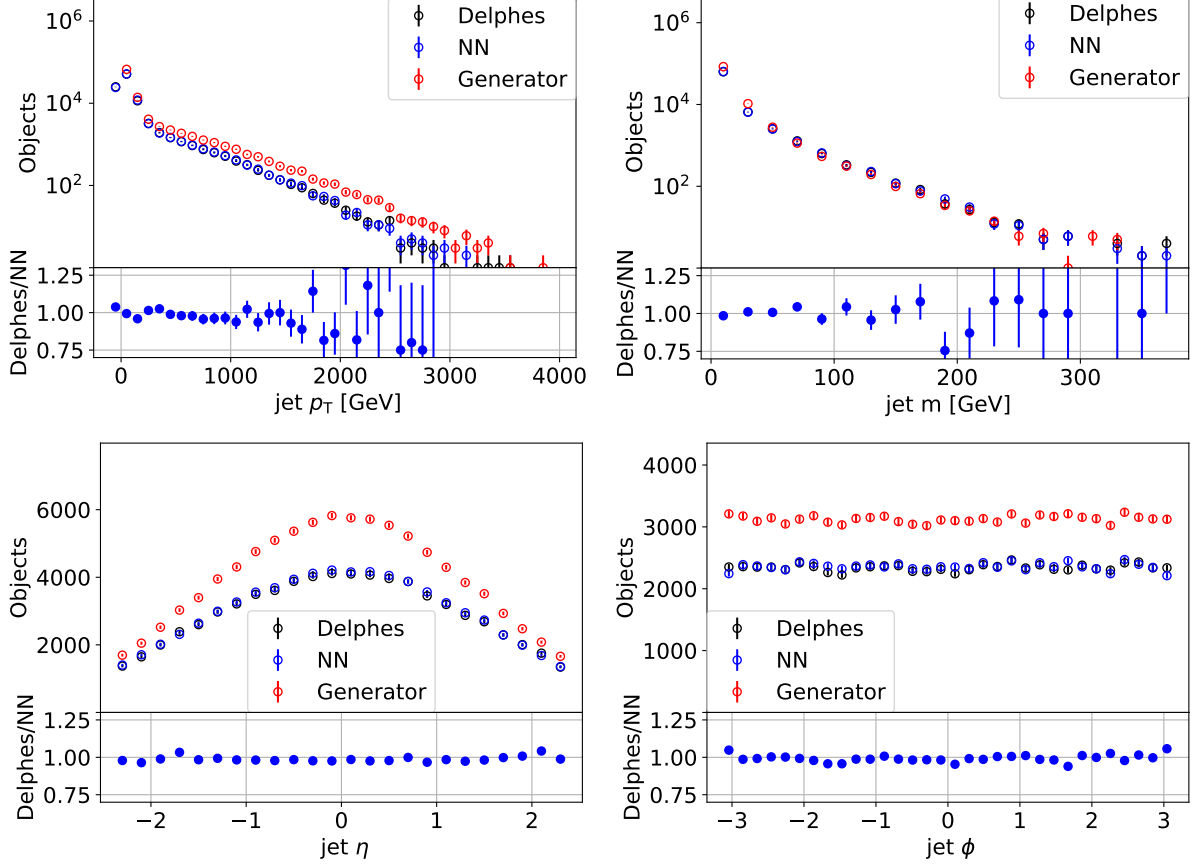


FIG. 6. NN-generated jet  $p_T$ , mass,  $\eta$ ,  $\phi$  compared to truth-level and detector-level jet features.

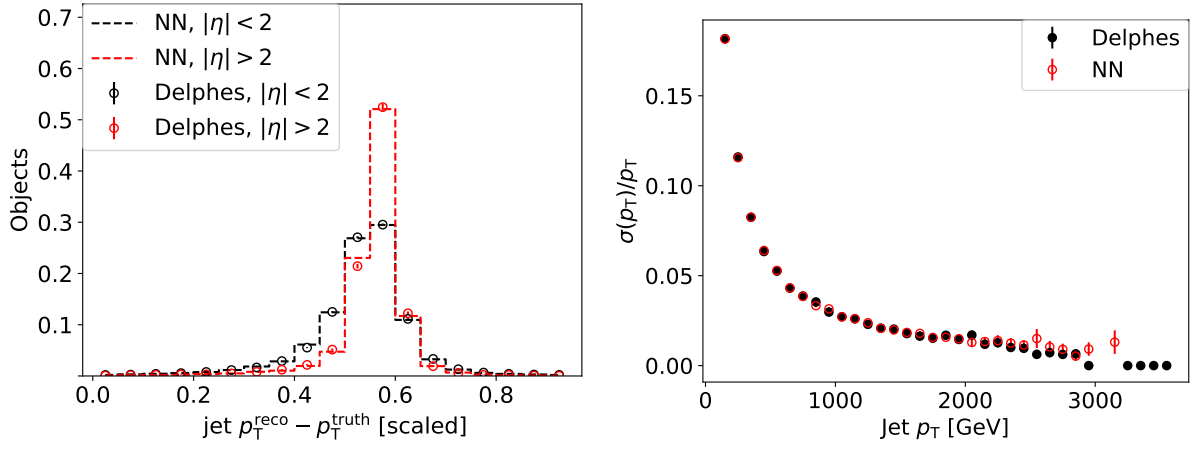


FIG. 7. Left: NN-generated jet  $p_T$  resolutions for central (black) and forward (red) jets for Delphes (circles) and NN-generated jets (dashed line). Right: The standard deviation of the  $p_T^{\text{truth}} - p_T^{\text{reco}}$  as a function of  $p_T$  for Delphes (black) and the NN (red).